

Journal Pre-proof

Measurement of solute permeability in the mouse spinal cord

Marlene Elisa Da Vitoria Lobo, David O Bates, Kenton P Arkill, Richard Philip Hulse



PII: S0165-0270(23)00099-7

DOI: <https://doi.org/10.1016/j.jneumeth.2023.109880>

Reference: NSM109880

To appear in: *Journal of Neuroscience Methods*

Received date: 27 February 2023

Revised date: 1 May 2023

Accepted date: 8 May 2023

Please cite this article as: Marlene Elisa Da Vitoria Lobo, David O Bates, Kenton P Arkill and Richard Philip Hulse, Measurement of solute permeability in the mouse spinal cord, *Journal of Neuroscience Methods*, (2023)
doi:<https://doi.org/10.1016/j.jneumeth.2023.109880>

This is a PDF file of an article that has undergone enhancements after acceptance, such as the addition of a cover page and metadata, and formatting for readability, but it is not yet the definitive version of record. This version will undergo additional copyediting, typesetting and review before it is published in its final form, but we are providing this version to give early visibility of the article. Please note that, during the production process, errors may be discovered which could affect the content, and all legal disclaimers that apply to the journal pertain.

© 2023 Published by Elsevier.

Measurement of solute permeability in the mouse spinal cord

^bMarlene Elisa Da Vitoria Lobo, ^{b,c} David O Bates, ^bKenton P Arkill and ^aRichard Philip Hulse*

^a School of Science and Technology, Nottingham Trent University, Nottingham, NG11 8NS,

^bDivision of Cancer and Stem Cells, School of Medicine, Biodiscovery Institute, University of Nottingham, Nottingham NG7 2UH, ^cCentre of Membrane and Protein and Receptors (COMPARE), University of Birmingham and University of Nottingham, Midlands, UK.

*Corresponding author

Corresponding Author Contact Details

Dr Richard P Hulse

Richard.Hulse@ntu.ac.uk

School of Science and Technology

New Hall Block

Nottingham Trent University

Clifton Lane

Nottingham

NG11 8NS

Richard.Hulse@ntu.ac.uk

Category: Original Article

Abstract

Background

Sensory perception and motor dexterity is coordinated by the spinal cord, which remains effective due to maintenance of neuronal homeostasis. This is stringently controlled by the blood spinal cord barrier. Therefore, the function of the spinal cord is susceptible to alterations in the microvessel integrity (e.g. vascular leakage) and/or perfusion (e.g. changes in blood flow).

New Method

Spinal cord solute permeability was measured in anaesthetised mice. The lumbar spinal cord vertebra were stabilised and a coverslip secured to allow fluorescent tracers of vascular function

and anatomy to be visualised in the vascular network. Fluorescence microscopy allowed real time measurements of vascular leakage and capillary perfusion within the spinal cord.

Results

Capillaries were identified through fluorescent labelling of the endothelial luminal glycocalyx (wheat germ agglutinin 555). Real time estimation of vascular permeability through visualisation of sodium fluorescein transport was recorded from identified microvessels in the lumbar dorsal horn of the spinal cord.

Comparison with Existing Method(s)

Current approaches have used histological and/or tracer based *in-vivo* assays alongside cell culture to determine endothelium integrity and/or function. These only provide a snapshot of the developing vasculopathy, restricting the understanding of physiological function or disease progression over time.

Conclusions

These techniques allow for direct visualisation of cellular and/or mechanistic influences upon vascular function and integrity, which can be applied to rodent models including disease, transgenic and/or viral approaches. This combination of attributes allows for real time understanding of the function of the vascular network within the spinal cord.

Keywords

spinal cord, intravital, permeability, endothelial cell,

1. Introduction

The nervous system consists of a wide degree of differing cellular phenotypes, which work together to control an integrated physiological system. The vasculature has a crucial role in the context of neurophysiology and neuropathology through providing essential provision of nutrients for neuronal survival and function. This includes delivery and removal of solutes to the neural tissues through blood perfusion from arterioles through small capillaries to post-capillary venules. Furthermore, it plays a pivotal role in protecting the nervous tissue from potential damage by preventing toxic agents or pathogens from invading the tissue (Beggs et al., 2010). There is an extensive cellular diversity within the vascular network in the nervous system, including cell types such as endothelial cells, pericytes, and astrocytes (Gordh et al., 2006; Bartanusz et al., 2011; Dias et al., 2018). It is becoming increasingly apparent that the health of this vascular system is involved with the pathogenesis of neurodegenerative disease, with damage to the spinal cord vasculature strongly correlating with neuronal damage such as in multiple sclerosis (Uchida et al., 2019; Kumar et al., 2020), Alzheimer's disease (Nortley et al., 2019; Korte et al., 2020) and stroke (Reeson et al., 2015; Taylor et al., 2015).

Disturbances in microvessel function are prominently, though not exclusively, associated with exacerbated vascular leakage in the spinal cord in neuropathological circumstances (e.g. multiple sclerosis (Fung et al., 2012) and motor impairment (e.g. spinal cord traumatic injury (Li et al., 2017) and in disturbances of nociceptive processing and resulting chronic pain (such as in arthritis, or traumatic injury (Costigan et al., 2009; Beggs et al., 2010). Typically, studies have investigated a breakdown in the integrity of the endothelium, which is subsequently attributed to increased levels of vascular permeability (Beggs et al., 2010) and tissue penetrance of invading cell types (Montague-Cardoso and Malcangio, 2021). This arises due to alteration in the endothelial junction proteins and/or secretion of enzymatic proteases from infiltrating and/or resident cell types (Echeverry et al., 2011; Lee et al., 2014; Slomnicki et al., 2020).

Most current approaches to investigate the blood spinal cord barrier focus on histological evaluation of spinal cord (ie through cell labelling, measure of tracer) from rodents, humans and transgenic/viral models (Beazley-Long et al., 2018; Uchida et al., 2019). Measurement of vascular leakage has been estimated using immunofluorescent based assays following infusion of fluorescently labelled agents in vivo, which can subsequently be identified by histology or by quantifying the amount of the solute that penetrates and accumulates in the tissue (Echeverry et al., 2011). Quantification of vascular permeability following infusion of a fluorescent tracer (e.g. TRITC conjugated dextran or albumin (Montague-Cardoso et al., 2020a; Da Vitoria Lobo et al., 2022), Evans' blue (Beggs et al., 2010; Hulse et al., 2015) or fluorescently labelled cell types (e.g. monocyte (Montague et al., 2018)) administered either via intravenous or systemic approaches can be evaluated (Beggs et al., 2010). These techniques provide information regarding how the structure of the microvessels networks are influenced by differing experimental interventions. However, they provide a single snapshot of the functionality and integrity of the spinal cord microvasculature.

Intravital imaging of nervous tissues (Cheng et al., 2019; Bakhsheshian et al., 2021) allows for acquisition of high resolution datasets of an array of cellular physiological responses such as vessel leakage, using a variety of experimental tools and sensors. Vessel architecture can be determined whilst simultaneously acquiring physiological measurements of vascular function such as vessel perfusion and permeability. Despite the physical difficulties of stabilising and accessing the spinal cord, in vivo imaging of the rodent spinal cord has recently been used by a number of groups to determine microvessel function in health and disease (Farrar et al., 2012; Sekiguchi et al., 2016; Montague-Cardoso et al., 2020b). Here we present an in vivo imaging methodology to estimate real time vessel permeability via leakage of fluorescent tracers in the spinal cord.

2. Materials

2.1. Ethical Approval and Animals used

All experiments involving animal were performed in accordance with the United Kingdom animals (Scientific procedures) Act 1986 and local ethical review board. Animals had *ad libitum* access to standard chow and housed under 12:12h light:dark conditions. All studies for immunohistochemistry (2 mice) and intravital imaging (10 mice) studies were performed in adult male C57.bl6 mice (25-30g; Charles River).

2.2. Immunohistochemistry

Adult male mice were anaesthetised and anaesthesia was maintained by intraperitoneal injection of a combination of Ketamine (50mg/kg) and Medetomidine hydrochloride (0.5mg/kg). Wheat germ agglutinin AlexaFluor conjugated 555 (WGA555, 4mg/kg, 100uL in sterile PBS per mouse, ThermoFisher Scientific, Inc cat no. W32464) was intravenously injected via the tail vein. 15 min post injection of WGA555, cardiac perfusion fixation was performed using 4% paraformaldehyde. The lumbar spinal cord was extracted, submerged in 4% formaldehyde and left overnight at 4°C. These samples were prepared for cryoprotection via submersion in 30% sucrose overnight at 4°C. Tissue was cryosectioned at 50µm thickness and mounted on superfrost plus slides or stored at -80 °C. Spinal cord sections were washed in phosphate-buffered saline (PBS) for 10 minutes on two occasions to remove debris that may impair cryosection imaging. This was subsequently followed by incubation with DAPI (made up in water) for 5 min in a hydration chamber at room temperature. A coverslip was mounted with Vectashield (Vector Laboratories) and slides were imaged on a confocal microscope (SP8, Leica), noting WGA555 excitation peak equates to 553 nm and emission peak at 568 nm.

2.3. Anaesthesia Induction and Laminectomy

Adult male mice were anaesthetised by intraperitoneal injection of a combination of Ketamine (50mg/kg) and Medetomidine hydrochloride (0.5mg/kg). Anaesthesia was regularly monitored for anaesthetic depth (e.g. foot and corneal reflex), with anaesthesia maintained via further intraperitoneal injections of Ketamine (50mg/kg) and Medetomidine hydrochloride (0.5mg/kg) where appropriate. Following anaesthesia induction mouse body temperature (~37°C) was maintained through a feedback control system using a heat pad and a rectal probe. Access to the spinal cord was performed via a laminectomy of the thoracic/lumbar region of the spinal cord. The skin on the dorsal surface of the mouse was shaved, all hair removed and the region cleaned/sterilised with chlorohexidine. An insertion along the vertebral column on the dorsal surface of the skin was made using a scalpel blade cut approximately 2 cm in length. Skin was separated from underlying tissues using blunt dissection. Exposed muscle and connective tissue were removed to expose the vertebrae and the vertebral processes. Vertebral processes were removed including transverse processes along with any remaining muscle and connective tissue

from the lateral aspects of the vertebrae. A laminectomy was performed between T12-L1 to expose the lumbar segments L3-L5 of the spinal cord. Damage to the dura was minimised. Following exposure of the spinal cord, the tissue was kept hydrated with sterile saline.

2.4. Intravital Spinal Cord Imaging Preparation

Following laminectomy an inhouse window chamber was assembled and attached to mouse spinal vertebra (Fig.1A-E) to allow maintenance of the tissue whilst allowing a robust imaging platform to perform the studies. The window chamber consists of two sets of side pillars and attachment bars that clamp either side of the vertebra. Here we rotated the spinal column to locate the dorsal horn. This provides a fixed configuration to enable secure attachment to the microscope allowing for stable image capture. The face plate for the window chamber, which possesses a recessed insert for a glass coverslip, is attached to the side pillars, holding the window chamber in position. A silicone elastomer (Kwik Sil, World Precision Instruments) is used to fill the gap in the face plate to immerse the spinal cord. A glass coverslip (diameter = 5mm, thickness = #0, Warner Instruments) is inserted into the recess in the face plate of the window chamber and pressed against the silicone elastomer. A bubble free seal was ensured and left to allow the elastomer to cure. If bubbles were present or coverslip not secure, the coverslip was removed and elastomer was reapplied with a new coverslip inserted. Following the positioning of the face plate, side pillars and covers slip, the attachment bars are screwed in position on an imaging frame to secure the spinal cord. This imaging frame allows the mouse to be positioned on the microscope on a bespoke physiological stage (Scientifica).

2.5. Intravital Imaging Fluorescent Vessel Labelling

To identify the endothelium in the spinal cord, AlexaFluor 555 conjugated wheat germ agglutinin, (WGA555, 4mg/kg, equating to a volume of 100uL in sterile PBS per mouse, ThermoFisher Scientific, Inc cat no. W32464) was intravenously injected via tail vein. The mouse was left for 15 min and positioned on the microscope stage and the spinal cord was imaged using an inverted confocal microscope (SP8, Leica Microsystems) with a bespoke physiological stage (Scientifica) to hold manipulators. At the imaging location the standard imaging plate slide holder was removed and a house built XZY stage with built in coverslip as outlined in 2.4. Confocal settings applied; emission wavelengths of the lasers utilized were 488 nm and 552 nm alongside a dry 10x objective with a NA 0.4. (HC PL APO CS). For image acquisition resolution was 512 x 512 at 0.37s per frame, with sodium fluorescein acquisition channel settings being Gain 625, Pinhole 1.68, Zoom 2.25, PMT 495-545. For WGA 555 acquisition channel settings were Gain 625, Zoom 2.25, PMT 567-618. The Individual vessels were identified as those that contained WGA555 labelled endothelium and were less than 20µm in diameter. Regions of vessel segment were identified that had no branch points along the length. This enabled offline analysis of solute permeability. Following identification of labelled vessels, permeability was

measured using sodium fluorescein (Sigma-Aldrich, cat no.1038870050, peak excitation 498nm, peak emission 512nm). Sodium fluorescein was administered at either 10mg/ml or 100mg/ml in sterile PBS via intraperitoneal injection. Immediately after sodium fluorescein injection, the spinal cord was imaged (minimum of 120s with a frame rate of 10 frames/s). All settings relating to the confocal laser configuration (e.g. gain and offset) were maintained for all experiments aligned to the study and illumination of tissue was maintained at a configuration that excluded blood vessel lumen fluorescence saturation.

2.6. Statistical Analysis of solute permeability and red blood cell velocity

All image processing was performed using Fiji (<https://imagej.net/Fiji>) (Schindelin et al., 2012), and GraphPad Prism v8 was used for data analysis. Data presented as mean \pm standard error of mean in figure 3E, whereas in figures 2F, 3B and 3C data is presented as mean. Acquired images were captured (.LIF) and exported as using Leica LAS software (acquired image precision of either 256 x 256 pixels or 512 x 512 pixels). These were converted into .TIFF file format. Using Fiji vessels radius (identified using WGA555 staining) was determined using a calibrated freehand tool. Analysis for measurement of permeability and red blood cell velocity (RBC) velocity over time, a region of the vessel lacking bifurcations and overlap of regions of interest between differing vessels was chosen. Vessel diameter was recorded by measuring across the segment of identified vessel and a plot profile was produced to evaluate fluorescence intensity. Vessel diameter was determined by measuring between the two fluorescent peaks, which identify vessel wall. Sodium fluorescein vessel leakage was measured using fluorescence intensity in a chosen region of interest (ROI) that spanned across the vessel wall; including fluorescein vessel intensity inside the vessel lumen and adjacent tissue outside the vessel wall. The fluorescence intensity in the adjacent tissue outside the vessel increased linearly over time. This allowed for initial sodium fluorescein permeability ($P_{NaF}^{t=0}$) to be calculated by EQ. 1 and illustrated (Fig. 3B) (Huxley et al., 1987):

$$P_{NaF}^{t=0} = \frac{r}{2\Delta I_f} \left(\frac{dI_f}{dt} \right) \quad \text{EQ.1}$$

Where

I_f = fluorescence intensity of ROI

r = radius of vessel

ΔI_f = fluorescence intensity from the luminal vessel fluorescein bolus

$\frac{dI_f}{dt}$ = rate of fluorescent intensity change from plateau over time (s).

It was not possible to determine the capillary hydrostatic pressure directly; however, the velocity was determined using kymographs of cell trafficking through the vessel of known radius. Velocity of blood flow was determined by imaging sodium fluorescein filled vessels to track RBC

movement along the vessel lumen. Unlabelled RBCs identified by shadows (areas of no fluorescent molecule in the lumen) were used to produce kymographs depicting x axis representing distance (Δd) and y axis represents time (Δt).

The velocity can be related to volumetric flow (F) as EQ2.

$$F = \frac{V_m}{2} \cdot \pi r^2 \quad \text{EQ.2}$$

Where V_m is the maximum velocity. Whilst full quantification is impossible, particularly with blood, F can be approximated by:

$$F \propto \left(\frac{\Delta H}{L}\right) r^4 \quad \text{EQ.3}$$

Where ΔH is the change in Hydrostatic pressure along the length (L) of vessel, i.e. $\frac{\Delta H}{L}$ is the hydrostatic pressure at the ROI. Therefore, if the proportionality of V_m to r^2 is constant then any changes in solute flux are most likely to be predominately changes in the permeability to the vessel wall rather than haemodynamic effect changing flow or hydrostatic pressure. Diagrams were created with BioRender.com.

Results

Real time measurement of vascular permeability in the spinal cord.

To enable identification of the vasculature in the spinal cord, fluorescence labelling was used to stain the endothelium (Betteridge et al., 2017). In spinal cord cryosections prepared from mice administered WGA555 (4mg/kg) via intravenous tail vein injection, the blood vessel endothelium was identified via WGA55 positive labelling in the dorsal horn of the spinal cord (Fig. 1F & G). To determine whether vessels could be imaged in vivo, anaesthetised mice were perfused with WGA555 and imaged in real time. Fig. 1H & I show endothelial staining of the spinal cord, which could be used to identify microvessels (arrows) for permeability measurement in the spinal cord. Following identification of the microvessel with WGA555 labelling (Fig. 2A), vessel permeability in the spinal cord was determined. Differing fluorescent tracers can be applied to interrogate vascular permeability. Previously sodium fluorescein has been adopted to investigate microvessel disturbances and alterations in solute permeability (Allen et al., 2020) Intraperitoneal injection of sodium fluorescein resulted in real time visualisation of perfusion (Fig. 2B, representative merge example Fig. 2C) (Allen et al., 2020). Post injection sodium fluorescein distribution in the vessel network of the spinal cord was acquired from 0s (point of injection; Fig. 2D) over 2 min (Fig. 2E), with sodium fluorescein administration delivered initially at either 10mg/ml or 100mg/ml (Fig. 2F; intraperitoneal). In all consequent follow up studies 100mg/ml was administered.

In an identified WGA555 labelled vessel (Fig. 3A), solute permeability was determined by measuring the fluorescence intensity in the ROI against time (Fig. 3A & 3B). Initially following sodium fluorescein administration, there was a rapid increase in fluorescence intensity within the vessel lumen, which plateaued and stabilised (Fig. 3A & B, ΔI_{f0}). Fluorescent intensity outside the vessel wall in the adjacent tissue increased in a linear manner (Fig. 3C, dI_f/dt), indicative of solute transport across the vessel wall. For measurement of solute permeability to meet the assumptions of no change in haemodynamics requires an assumption of undisturbed hydrostatic pressure and constant vessel cross sectional area. Hydrostatic pressure was assumed to be constant as there were no fluctuations in red blood vessel velocity (Fig. 3E) or identified vessel diameter across a known length of capillary (Fig. 3F). Sodium fluorescein permeability was determined to be $6.3 \times 10^{-8} \text{cm.s}^{-1}$. This is comparable to other investigations of solute permeability measures within the central nervous system (brain) in rats utilising optical imaging ($1.6810^{-8} \text{cm.s}^{-1}$ - $2.4510^{-6} \text{cm.s}^{-1}$) (Yuan et al., 2009; Shi et al., 2014; Shin et al., 2020).

Discussion

Here we describe a method to determine vascular permeability of spinal cord vessels in real time. Experimental approaches to date have typically relied upon inherently time locked studies (ie histological evaluation of tracer tissue penetration), which only provide a snapshot of the systems in play in relation to vessel function though offering insights into the concept of increased vascular permeability.

The approach presented here takes advantage of advances in optical imaging to measure vessel function, in real time, principally focussing upon vascular permeability in this instance. The endothelium is a semi-permeable barrier that coordinates tissue homeostasis through the movement of molecules and cells transported in the blood across the endothelium. This methodological approach enables researchers to measure functional activity of the vessel under in vivo physiological pressures and blood flow. Current approaches provide an advancement of our understanding of the role that the blood spinal cord barrier (BSCB) plays in maintaining spinal cord homeostasis and in the development of neuropathology, but lack the methodological resolution to fully appreciate the molecular and physiological impact upon the BSCB. The current approach allows pharmacological intervention to modulate vessel function and immediate measurement of experimental data from point of experimental intervention until termination of the study.

As highlighted, vessel permeability is the physiological process that is determined by net capillary differences across a membrane of solute and water whilst considering the impact of hydrostatic pressure (Michel and Curry, 1999; Curry and Adamson, 2010). Furthermore, vessel structural parameters including interjunctional proteins (e.g. Claudin, Occludin, Zonula Occludens 1) and an endothelium luminal carbohydrate rich filter known as the glycocalyx are also factors of consideration when determining molecular insights into vessel permeability (Curry and Adamson, 2010; Betteridge et al., 2017). Using intravital imaging in rodents allows for the evaluation of molecular transport across the endothelial wall. Using fluorescent labelling the structural context of the luminal vessel lining can be identified as presented using different fluorochromes or conjugated antibodies as well as differing sized fluorescent tracers. Furthermore, transgenic models (Montague-Cardoso et al., 2020a) and/or viral approaches (Dogbevia et al., 2020) could also be incorporated to provide a fuller representative of the system investigated. This is whilst allowing for the tracking of solute movement across the endothelial membrane using a fluorochrome tagged molecule to measure solute permeability.

Here we present an approach that allows simultaneous measurement of multiple physiological processes in relation to an identified capillary, including blood flow, cell trafficking, vessel diameter and permeability. In addition, these imaging approaches also enables the possibility of

increasing the number of vessels that data is acquired from in any one instance. Regions of interest can be considered to expand analysis across multiple vessel segments.

Conclusion

This approach allows the direct measurement of vessel permeability in the spinal cord to investigate related aspects of health and disease.

Journal Pre-proof

Acknowledgements

RPH and MD performed the experimental work. RPH, MD, KA and DOB contributed to the conception or design of the work in addition to acquisition, analysis or interpretation of data for the work. RPH, MD, KA and DOB drafted the work or revised it critically for important intellectual content. RPH drafted the manuscript with contributions from all authors. All authors approved the final version of the manuscript, agree to be accountable for all aspects of the work in ensuring that questions related to the accuracy or integrity of any part of the work are appropriately investigated and resolved all persons designated as authors qualify for authorship, and all those who qualify for authorship are listed. We would like to acknowledge Prof Chris Schaffer at Cornell University for his advice.

Funding

This work was supported by the European Foundation for the Study of Diabetes Microvascular Programme supported by Novartis to RPH (Nov 2015_2 to RPH), the EFSD/Boehringer Ingelheim European Research Programme in Microvascular Complications of Diabetes (BI18_5 to RPH), and the Rosetree Trust (A1360 to RPH).

References

- Allen, C.L., Malhi, N.K., Whatmore, J.L., Bates, D.O., Arkill, K.P., 2020. Non-invasive measurement of retinal permeability in a diabetic rat model. *Microcirculation* e12623. <https://doi.org/10.1111/micc.12623>
- Bakhsheshian, J., Strickland, B.A., Mack, W.J., Zlokovic, B. v., 2021. Investigating the blood–spinal cord barrier in preclinical models: a systematic review of in vivo imaging techniques. *Spinal Cord*. <https://doi.org/10.1038/s41393-021-00623-7>
- Bartanusz, V., Jezova, D., Alajajian, B., Digicaylioglu, M., 2011. The blood-spinal cord barrier: Morphology and clinical implications. *Ann Neurol*. <https://doi.org/10.1002/ana.22421>
- Beazley-Long, N., Moss, C.E., Ashby, W.R., Bestall, S.M., Almahasneh, F., Durrant, A.M., Benest, A.V., Blackley, Z., Ballmer-Hofer, K., Hirashima, M., Hulse, R.P., Bates, D.O., Donaldson, L.F., 2018. VEGFR2 promotes central endothelial activation and the spread of pain in inflammatory arthritis. *Brain Behav Immun*. <https://doi.org/10.1016/j.bbi.2018.03.012>
- Beggs, S., Liu, X.J., Kwan, C., Salter, M.W., 2010. Peripheral nerve injury and TRPV1-expressing primary afferent C-fibers cause opening of the blood-brain barrier. *Mol Pain* 6, 74. <https://doi.org/10.1186/1744-8069-6-74>
- Betteridge, K.B., Arkill, K.P., Neal, C.R., Harper, S.J., Foster, R.R., Satchell, S.C., Bates, D.O., Salmon, A.H.J., 2017. Sialic acids regulate microvessel permeability, revealed by novel in vivo studies of endothelial glycocalyx structure and function. *Journal of Physiology*. <https://doi.org/10.1113/JP274167>
- Cheng, Y.T., Lett, K.M., Schaffer, C.B., 2019. Surgical preparations, labeling strategies, and optical techniques for cell-resolved, in vivo imaging in the mouse spinal cord. *Exp Neurol*. <https://doi.org/10.1016/j.expneurol.2019.05.010>
- Costigan, M., Moss, A., Latremoliere, A., Johnston, C., Verma-Gandhu, M., Herbert, T.A., Barrett, L., Brenner, G.J., Vardeh, D., Woolf, C.J., Fitzgerald, M., 2009. T-cell infiltration and signaling in the adult dorsal spinal cord is a major contributor to neuropathic pain-like hypersensitivity. *J Neurosci* 28, 14415–14422.
- Curry, F.R.E., Adamson, R.H., 2010. Vascular permeability modulation at the cell, microvessel, or whole organ level: Towards closing gaps in our knowledge. *Cardiovasc Res* 87, 218–229. <https://doi.org/10.1093/cvr/cvq115>
- Da Vitoria Lobo, M.E., Weir, N., Hardowar, L., Al Ojaimi, Y., Madden, R., Gibson, A., Bestall, S.M., Hirashima, M., Schaffer, C.B., Donaldson, L.F., Bates, D.O., Hulse, R.P., 2022. Hypoxia induced carbonic anhydrase mediated dorsal horn neuron activation and induction of neuropathic pain. *Pain* 163, 2264–2279. <https://doi.org/10.1097/j.pain.0000000000002627>
- Dias, D.O., Kim, H., Holl, D., Werne Solnestam, B., Lundeberg, J., Carlen, M., Goritz, C., Frisen, J., 2018. Reducing Pericyte-Derived Scarring Promotes Recovery after Spinal Cord Injury. *Cell* 173, 153–165 e22. <https://doi.org/10.1016/j.cell.2018.02.004>
- Dogbevia, G., Grasshoff, H., Othman, A., Penno, A., Schwaninger, M., 2020. Brain endothelial specific gene therapy improves experimental Sandhoff disease. *Journal of Cerebral Blood Flow and Metabolism* 40, 1338–1350. <https://doi.org/10.1177/0271678X19865917>

- Echeverry, S., Shi, X.Q., Rivest, S., Zhang, J., 2011. Peripheral nerve injury alters blood-spinal cord barrier functional and molecular integrity through a selective inflammatory pathway. *J Neurosci* 31, 10819–10828. <https://doi.org/10.1523/JNEUROSCI.1642-11.2011>
- Farrar, M.J., Bernstein, I.M., Schlafer, D.H., Cleland, T.A., Fetcho, J.R., Schaffer, C.B., 2012. Chronic in vivo imaging in the mouse spinal cord using an implanted chamber. *Nat Methods* 9, 297–302. <https://doi.org/10.1038/nmeth.1856>
- Fung, A., Vizcaychipi, M., Lloyd, D., Wan, Y., Ma, D., 2012. Central nervous system inflammation in disease related conditions: mechanistic prospects. *Brain Res* 1446, 144–155. <https://doi.org/10.1016/j.brainres.2012.01.061>
- Gordh, T., Chu, H., Sharma, H.S., 2006. Spinal nerve lesion alters blood-spinal cord barrier function and activates astrocytes in the rat. *Pain* 124, 211–221. <https://doi.org/10.1016/j.pain.2006.05.020>
- Hulse, R.P., Beazley-Long, N., Ved, N., Bestall, S.M., Riaz, H., Singhal, P., Hofer, K.B., Harper, S.J., Bates, D.O., Donaldson, L.F., 2015. Vascular endothelial growth factor-A¹⁶⁵ prevents diabetic neuropathic pain and sensory neuronal degeneration. *Clin Sci* 129. <https://doi.org/10.1042/CS20150124>
- Huxley, V.H., Curry, F.E., Adamson, R.H., 1987. Quantitative fluorescence microscopy on single capillaries: α -lactalbumin transport. *Am J Physiol Heart Circ Physiol* 252. <https://doi.org/10.1152/ajpheart.1987.252.1.h188>
- Korte, N., Nortley, R., Attwell, D., 2020. Cerebral blood flow decrease as an early pathological mechanism in Alzheimer's disease. *Acta Neuropathol*. <https://doi.org/10.1007/s00401-020-02215-w>
- Kumar, Vinod., Lee, J.D., Coulson, E.J., Woodruff, T.M., 2020. A validated quantitative method for the assessment of neuroprotective barrier impairment in neurodegenerative disease models. *J Neurochem*. <https://doi.org/10.1111/jnc.15119>
- Lee, J.Y., Choi, H.Y., Ahn, H.J., Ju, B.G., Yune, T.Y., 2014. Matrix metalloproteinase-3 promotes early blood-spinal cord barrier disruption and hemorrhage and impairs long-term neurological recovery after spinal cord injury. *American Journal of Pathology*. <https://doi.org/10.1016/j.ajpath.2014.07.016>
- Li, Y., Lucas-Osma, A.M., Black, S., Bandet, M. V., Stephens, M.J., Vavrek, R., Sanelli, L., Fenrich, K.K., Di Narzo, A.F., Dracheva, S., Winship, I.R., Fouad, K., Bennett, D.J., 2017. Pericytes impair capillary blood flow and motor function after chronic spinal cord injury. *Nat Med* 23, 733–741. <https://doi.org/10.1038/nm.4331>
- Michel, C.C., Curry, F.E., 1999. Microvascular permeability. *Physiol Rev* 79, 703–761. <https://doi.org/10.1152/physrev.1999.79.3.703>
- Montague, K., Simeoli, R., Valente, J., Malcangio, M., 2018. A novel interaction between CX3CR1 and CCR2 signalling in monocytes constitutes an underlying mechanism for persistent vincristine-induced pain. *J Neuroinflammation*. <https://doi.org/10.1186/s12974-018-1116-6>
- Montague-Cardoso, K., Malcangio, M., 2021. Changes in blood–spinal cord barrier permeability and neuroimmune interactions in the underlying mechanisms of chronic pain. *Pain Rep* 6, e879. <https://doi.org/10.1097/PR9.0000000000000879>

- Montague-Cardoso, K., Pitcher, T., Chisolm, K., Salera, G., Lindstrom, E., Hewitt, E., Solito, E., Malcangio, M., 2020a. Changes in vascular permeability in the spinal cord contribute to chemotherapy-induced neuropathic pain. *Brain Behav Immun* 83, 248–259. <https://doi.org/10.1016/j.bbi.2019.10.018>
- Montague-Cardoso, K., Pitcher, T., Chisolm, K., Salera, G., Lindstrom, E., Hewitt, E., Solito, E., Malcangio, M., 2020b. Changes in vascular permeability in the spinal cord contribute to chemotherapy-induced neuropathic pain. *Brain Behav Immun*. <https://doi.org/10.1016/j.bbi.2019.10.018>
- Nortley, R., Korte, N., Izquierdo, P., Hirunpattarasilp, C., Mishra, A., Jaunmuktane, Z., Kyrargyri, V., Pfeiffer, T., Khennouf, L., Madry, C., Gong, H., Richard-Loendt, A., Huang, W., Saito, T., Saido, T.C., Brandner, S., Sethi, H., Attwell, D., 2019. Amyloid beta oligomers constrict human capillaries in Alzheimer's disease via signaling to pericytes. *Science (1979)* 365. <https://doi.org/10.1126/science.aav9518>
- Reeson, P., Tennant, K.A., Gerrow, K., Wang, J., Weiser Novak, S., Thompson, K., Lockhart, K.L., Holmes, A., Nahirney, P.C., Brown, C.E., 2015. Delayed inhibition of VEGF signaling after stroke attenuates blood-brain barrier breakdown and improves functional recovery in a comorbidity-dependent manner. *J Neurosci* 35, 5128–5143. <https://doi.org/10.1523/JNEUROSCI.2810-14.2015>
- Schindelin, J., Arganda-Carreras, I., Frise, E., Kaynig, V., Longair, M., Pietzsch, T., Preibisch, S., Rueden, C., Saalfeld, S., Schmid, B., Tinevez, J.Y., White, D.J., Hartenstein, V., Eliceiri, K., Tomancak, P., Cardona, A., 2012. Fiji: an open-source platform for biological-image analysis. *Nat Methods* 9, 676–682. <https://doi.org/10.1038/nmeth.2019>
- Sekiguchi, K.J., Shekhtmeyster, P., Merten, K., Arena, A., Cook, D., Hoffman, E., Ngo, A., Nimmerjahn, A., 2016. Imaging large-scale cellular activity in spinal cord of freely behaving mice. *Nat Commun*. <https://doi.org/10.1038/ncomms11450>
- Shi, L., Zeng, M., Fu, B.M., 2014. Temporal effects of vascular endothelial growth factor and 3,5-cyclic monophosphate on blood-brain barrier solute permeability in vivo. *J Neurosci Res* 92, 1678–1689. <https://doi.org/10.1002/jnr.23457>
- Shin, D.W., Fan, J., Luu, E., Khalid, W., Xia, Y., Khadka, N., Bikson, M., Fu, B.M., 2020. In Vivo Modulation of the Blood–Brain Barrier Permeability by Transcranial Direct Current Stimulation (tDCS). *Ann Biomed Eng* 48, 1256–1270. <https://doi.org/10.1007/s10439-020-02447-7>
- Slomnicki, L.P., Myers, S.A., Saraswat Ohri, S., Parsh, M. V., Andres, K.R., Chariker, J.H., Rouchka, E.C., Whittemore, S.R., Hetman, M., 2020. Improved locomotor recovery after contusive spinal cord injury in *Bmal1* $-/-$ mice is associated with protection of the blood spinal cord barrier. *Sci Rep*. <https://doi.org/10.1038/s41598-020-71131-6>
- Taylor, S.L., Trudeau, D., Arnold, B., Wang, J., Gerrow, K., Summerfeldt, K., Holmes, A., Zamani, A., Brocardo, P.S., Brown, C.E., 2015. VEGF can protect against blood brain barrier dysfunction, dendritic spine loss and spatial memory impairment in an experimental model of diabetes. *Neurobiol Dis* 78, 11.
- Uchida, Y., Sumiya, T., Tachikawa, M., Yamakawa, T., Murata, S., Yagi, Y., Sato, K., Stephan, A., Ito, K., Ohtsuki, S., Couraud, P.O., Suzuki, T., Terasaki, T., 2019. Involvement of Claudin-11 in

Disruption of Blood-Brain, -Spinal Cord, and -Arachnoid Barriers in Multiple Sclerosis. *Mol Neurobiol.* <https://doi.org/10.1007/s12035-018-1207-5>

Yuan, W., Lv, Y., Zeng, M., Fu, B.M., 2009. Non-invasive measurement of solute permeability in cerebral microvessels of the rat. *Microvasc Res* 77, 166–173. <https://doi.org/10.1016/j.mvr.2008.08.004>

Journal Pre-proof

Figure Legends

Figure 1 - Spinal cord microvessel fluorescent labelling of the endothelium in the mouse spinal cord

[A] Representative image of the window chamber in situ plus glass coverslip and silicone elastomer in place. Diagrams of the [B] compartments for the window chamber; side pillars, attachment bars, face plate and imaging frame, [C & D] positioned across the exposed spinal cord. [E] Diagrams demonstrates the spinal cord held within the window chamber and inverted on the objective. Cryosectioned lumbar [F] coronal brain and [G] spinal cord sections (50 μ m) were prepared from adult C57.bl6 mice injected with Wheat Germ Agglutinin Alexafluor 555 (4mg/kg), delivered via intravenous tail vein injection. WGA labelled endothelium in the central nervous system was visualised allowing identification of the blood vessels in the spinal cord (scale bar = 100 μ m). [H & I] In an anaesthetised adult C57.bl6 mouse the window chamber was assembled and Wheat Germ Agglutinin Alexafluor 555 (4mg/kg) was administered via intravenous tail vein injection. Confocal microscopy was used to visualise WGA555 labelled microvessels in the spinal cord in real time in the adult mouse.

Figure 2 – Fluorescent intensity of sodium fluorescein in spinal cord microvessels

Mouse injected intravenously via the tail vein with Wheat Germ Agglutinin Alexafluor 555 (4mg/kg) to allow visualisation of microvessels in the spinal cord in vivo via intravital imaging. To measure vessel permeability sodium fluorescein was injected via intraperitoneal injection. Representative example of a [A] WGA 555 labelled (Red) vessels (arrows) in the spinal cord and [B] sodium fluorescein perfused (Green; Overlay provided in [C]). Representative images of spinal cord microvessels following intraperitoneal injection of 100mg/ml sodium fluorescein at Time [D] 0s and [E] 120s demonstrating vessels are perfused with sodium fluorescein by 120s. [F] fluorescence intensity in the region of interest (ROI) over time for 10mg/ml and 100mg/ml Sodium fluorescein.

Figure 3 - Sodium fluorescein permeability quantification

[A] A region of interest (ROI) was identified across an identified vessel labelled with WGA555 (scale bar = 200 μ m). Sodium fluorescein is injected by intraperitoneal injection and fills the vessel lumen over 120s. [B] fluorescence intensity was displayed over time demonstrating a steep rate of increase fluorescence intensity in the region of interest (ROI), with initial fluorescence intensity change (ΔI_t) depicting change from T=0s to fluorescence intensity plateau (approximately 60s). Subsequent rate of increase in fluorescence intensity represents vessel leakage of sodium fluorescein over time (dI_t/dt). [C] Fluorescence intensity of sodium fluorescein in the vessel lumen (black) over time depicting steep rate of increase until plateau accompanied by a linear increase in fluorescence intensity in the adjacent tissue outside the vessel wall (grey). [D] Kymograph depicting unaltered trajectory of blood cell movement through a vessel

highlighting no change in vessel diameter or red blood cell velocity and [E] no change in vessel diameter.

Table 1 – Comparison of solute permeability measures across the central nervous system Here reference is made to differing measures of solute permeability in differing rodents and aspects of the central nervous system depicting solute tracer used and actual measure of solute permeability.

Reference	Central Nervous System Location	Rodent	Solute Tracer	Measure of Sodium Fluorescein Permeability (P^{NaF}, cm/s)
Hulse et al. 2022	Spinal Cord	C57/bl6Mouse, Male	Sodium Fluorescein	6.37×10^{-8}
Shin et al. 2020	Brain	Sprague Dawley Rat, Female	Sodium Fluorescein	1.68×10^{-8}
Ling Yan et al. 2014	Brain	Sprague Dawley Rat, Female	Sodium Fluorescein	1.89×10^{-8}
Wei Yuan et al. 2010	Brain	Sprague Dawley Rat, Female	Sodium Fluorescein	2.45×10^{-6}

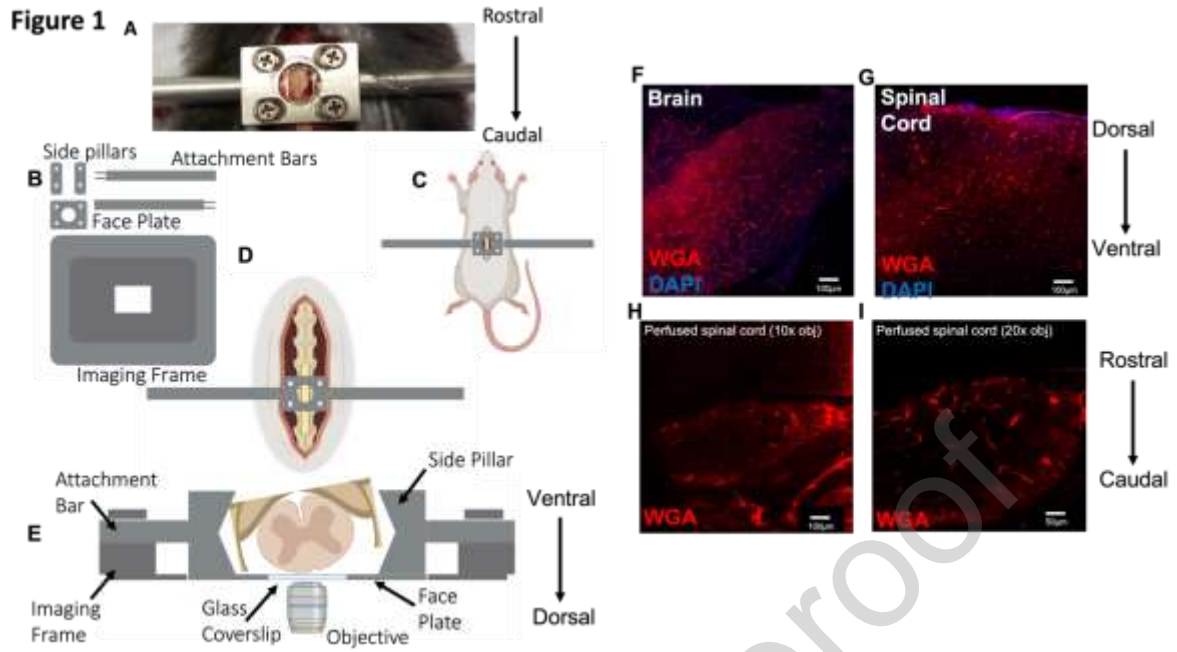


Figure 2

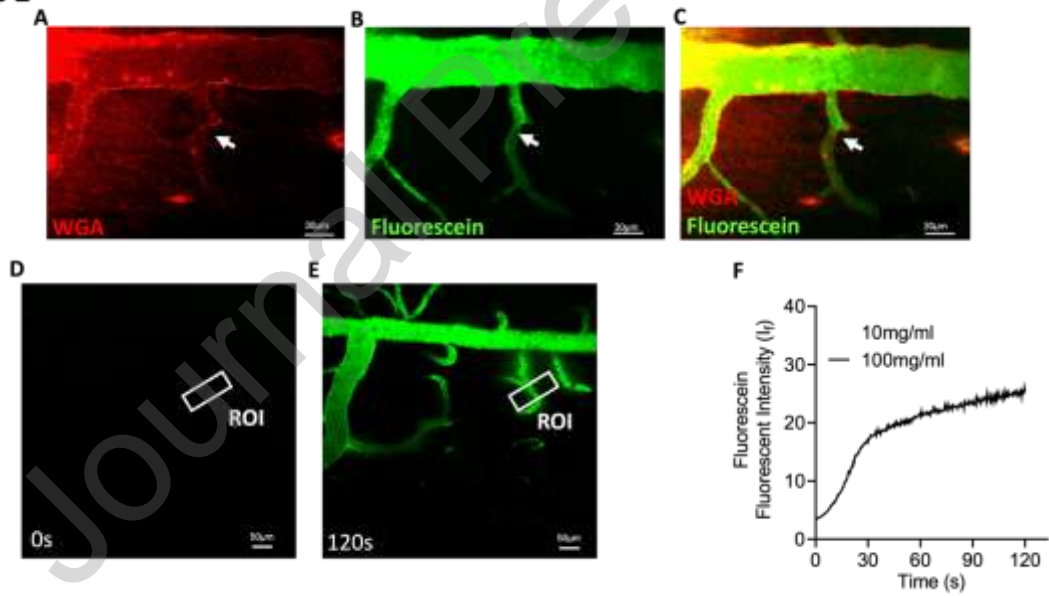
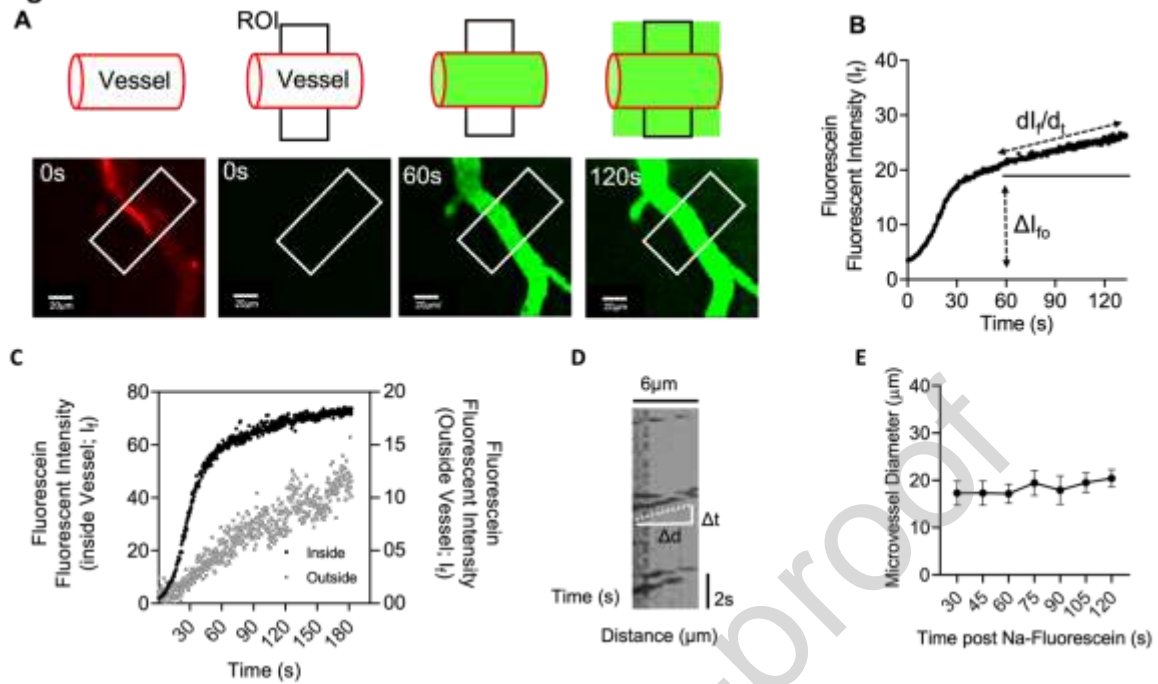


Figure 3



Highlights

- Intravital imaging of fluorescent tracers in perfused microvessels allows architectural components to be measured.
- Using fluorescent tracers in perfused microvessels allows architectural components of the blood spinal cord vessel network to be measured under physiological pressures.
- Real time measures of capillary functionality can be acquired allowing evaluation of cell trafficking and vessel permeability.

Credit author statement

Marlene Elisa Da Vitoria Lobo

Conceptualization, Methodology, Validation, Formal analysis, Investigation, Writing - Original Draft, Writing - Review & Editing, Visualization

David O Bates

Conceptualization, Methodology, Validation, Formal analysis, Investigation, Writing - Original Draft, Writing - Review & Editing, Visualization, Funding acquisition

Kenton P Arkill

Conceptualization, Methodology, Validation, Formal analysis, Investigation, Writing - Original Draft, Writing - Review & Editing, Visualization, Funding acquisition

Richard Philip Hulse

Conceptualization, Methodology, Validation, Formal analysis, Investigation, Writing - Original Draft, Writing - Review & Editing, Visualization, Supervision, Project administration, Funding acquisition

Declarations of interest

none

Highlights

- Intravital imaging allows evaluation of the function and anatomy of the mouse vasculature in the spinal cord.
- Using fluorescent tracers in perfused microvessels allows architectural components of the blood spinal cord vessel network to be measured under physiological pressures.
- Real time measures of capillary functionality can be acquired allowing evaluation of cell trafficking and vessel permeability.